Chemical Engineering Science 101 (2013) 865–877

Contents lists available at ScienceDirect

Chemical Engineering Science

journal homepage: www.elsevier.com/locate/ces

Evaporation dynamics of microbubbles ☆

William B. Zimmerman *, Mahmood K.H. Al-Mashhadani, H.C. Hemaka Bandulasena

Department of Chemical and Biological Engineering and Kroto Research Institute, Mappin Street, University of Sheffield, Sheffield S1 3JD, UK

HIGHLIGHTS

- Direct contact microbubble evaporation always achieves 100% relative humidity.
- Vapour temperature *reduction* with contact time increase.
- Absolute humidity *decrease* with contact time increase.
- Practically isothermal operation with low contact times.
- Greater than 95% selectivity for vaporization over sensible heat transfer achievable.

ARTICLE INFO

Article history:
Received 26 December 2012
Received in revised form
9 May 2013
Accepted 14 May 2013
Available online 30 May 2013

Keywords:
Microbubbles
Fluidics
Evaporation
Heat transfer
Distillation
Direct contact evaporation

ABSTRACT

Until recently, generating clouds of microbubbles was a relatively expensive proposition, with the smallest bubbles requiring high energy density from either the saturation–nucleation mechanism or Venturi effect. Due to the expense of processing with microbubbles, exploration of the acceleration effects of microbubbles for physico-chemical processes are largely unstudied, particularly those that are combined effects. In this paper, the trade-off between heat transfer and evaporation on the microbubble interface are explored, largely by computational modelling but supported by some experimental evidence. The hypothesis is that both processes are inherently transient, but that during short residence times, vaporization is favoured, while at longer residence times, sensible heat transfer dominates and results in re-condensation of the initially vaporized liquid. The computational model address how thin a layer thickness will result in the maximum absolute vaporization, after which sensible heat transfer condenses the vapour as the bubble cools. This maximum vaporization layer thickness is estimated to be a few hundred microns, on the order of a few microbubble diameters at most. If the maximum vaporization estimate and the contact time necessary to achieve it are accurately estimated, these are engineering design features needed to design a vaporizing system to achieve maximum removal of vapour with minimum heat transfer. The modelling work presented here should be considered in light of the humidification experiments also conducted which showed the exit air at 100% saturation, but increasing gas temperature with decreasing layer height, and decreasing water temperature with decreasing layer height, all of which are consistent with the predictions of the computational model.

1. Introduction

Why do we boil liquid to create water vapour? There are three effects achieved by boiling: (i) provision of the latent heat of vaporization, (ii) raising the temperature of the liquid so that the temperature of the vapour that is in equilibrium rises, hence raising the saturation pressure of water vapor or the absolute humidity achievable, (iii) increasing the gas–liquid interfacial area so as to increase the rate of evaporation. So if the aim is vaporization, most of the applied heat is actually used to raise the water temperature, rather than to "pay" for the latent heat of vaporization and to raise the absolute level of humidity achievable. This is an unavoidable consequence of equilibrium.

Direct contact evaporators (DCE) using superheated bubbles sparged into bubble columns have been known for many years, with the first English patent in 1887, and have recently been reviewed by Ribeiro and Lage (2005). Commonly, DCE is industrially implemented with spargers made from perforated plates generating fine (1–2 mm diameter) to coarse (~1 cm diameter) bubbles in turbulent flow. One of the major advantages for DCE is sensible heat transfer, which is reported to achieve 95% efficiencies and only a 2–5 °C difference in temperature between the bubble

* Corresponding author. Tel.: +44 114 222 7517; fax: +44 114 222 7501.
E-mail addresses: w.zimmerman@shef.ac.uk, w.zimmerman@sheffield.ac.uk (W.B. Zimmerman).

0009-2509/$ - see front matter © 2013 Elsevier. Published by Elsevier Ltd. All rights reserved.
http://dx.doi.org/10.1016/j.ces.2013.05.026

phase and the liquid. DCE is widely adopted for concentration of aqueous solutions, but does have a well known issue with potential foaming to contend with.

This article addresses the question whether a radically different approach can achieve more vaporization by conducting the process far from equilibrium. Can the same objectives of boiling be achieved without heating the liquid to equilibrium? Rather than heat the liquid, why not heat the gas phase? Since $\rho\, c_p$ for water is 3 orders of magnitude larger than that for gas, it is possible to raise the gas temperature very high with the same quanta of heat energy. Introducing the gas phase as a uniform cloud of microbubbles (Zimmerman et al., 2008, 2009, 2011) which are nearly monodisperse, and hence non-convergent (see Fig. 1), should increase the gas–liquid interfacial area which is expected to accelerate both sensible heat transfer and evaporation rates, as the typical models for rate laws for these processes are proportional to gas–liquid surface area. But which molecular mechanism – sensible heat transfer or evaporation – is favoured with microbubble dynamics? Even if they are equally important, there should be an exploitable effect: with heating of the liquid phase in traditional, equilibrium based vaporization, very little temperature rise is achieved due to the ratios of liquid to gas densities and heat capacities, hence practically no vaporization will be achieved by a quanta of heat transferred to the liquid. If half of the quanta of heat is used for vaporization and half for sensible heat transfer to the liquid, substantially more vaporization is achieved. Given the three orders of magnitude greater $\rho\, c_p$ for water than gas, it is clear that even a few percent of the heat used for vaporization will achieve more than an order of magnitude more vaporization than that same quanta of heat transmitted to the liquid at equilibrium.

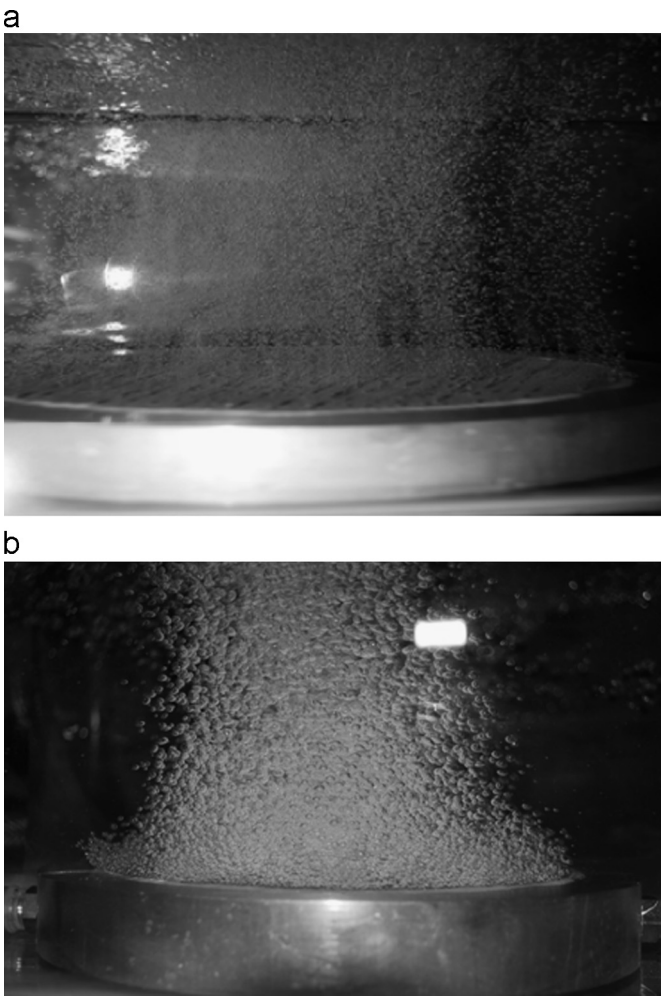

Fig. 1. Microporous diffuser with fluidic oscillation (a) and without (b) with nominally the same volumetric flow rate. The microbubbles are uniformly spaced and emerge at approximately the pore size with appropriately tuned oscillation frequency, and are therefore practically non-convergent. With steady flow, the bubbles emerge much larger and then, due to random release, coalesce with neighboring bubbles.

We have conducted preliminary experiments with microbubble heat transfer and vaporization that indicate that the absolute level of humidification is a controllable parameter, and varies significantly with the layer depth that the bubble rises through. Intuitively, one would think that the longer the residence time, the greater the vaporization achieved, as well as the greater the sensible heat transfer. This article addresses that "straw man" hypothesis and explains why the experiments achieve counter-intuitive control by varying the layer depth. The computational model is inherently transient, and demonstrates that transient operation, far from equilibrium, permits the selection for preferentially high absolute vaporization levels. It should be stressed that the purpose of the modelling is to characterize the contact time needed to achieve evaporation and heat transfer within the microbubble regime for design purposes, given that this is the first approach to the subject.

To our knowledge, these are the first experiments on humidification–dehumidification cycling by bubbles. However, two recent studies have considered coarse bubbles humidification–dehumidification dynamics: Narayan et al. (2013) builds on earlier experimental work (Narayan et al., 2011) but with bubbles of greater than 3 mm in size with heat transfer coefficients treated by correlation.

This paper is organized as follows. In Section 2, the numerical analysis is presented, along with computational modelling predictions for maximum humidification rates and residence times with maximum humidity. In Section 3, the only unknown modelling parameter, the microbubble heat transfer coefficient, is analyzed in respect of bubble column heat transfer/humidification experiments which motivated the numerical analysis. Section 4 holds the discussion and interpretation. In Section 5, conclusions are drawn and recommendations are proposed.

2. Model for evaporation from a rising microbubble

In this section we propose an idealized model based on imposed internal bubble flow with interfacial dynamics for heat and mass transfer treated phenomenologically, i.e. no external dynamics, which is appropriate for an isolated bubble or a dilute volume fraction of bubbles that are uniformly sized and spaced. This is intended as a single bubble model for the dynamics of fluidic oscillator induced microbubbles such as in Fig. 1(a). The previous models of superheated bubbles formed and rising in a direct contact evaporator by Campos and Lage (2000a, 2000b, 2001) do not take into account the internal gas dynamics of the bubble, so the model presented here can be considered complementary, as it uses phenomenological approaches to external dynamics and distributed system partial differential equations for heat and mass transport internally, with convection imposed. Ribeiro and Lage (2004a, 2004b) measured bubble size distributions in agreement with their formation and ascension model, demonstrating distributions larger than fine bubbles and into the coarse bubble regime. This model aims to treat submillimeter bubbles primarily.

2.1. Model equations

The modelling approach adopted here is to assume that all bubbles are sufficiently small that surface tension opposes deformation from a spherical shape, and that the time to achieve fully developed laminar flow is infinitesimally short after bubble

injection and release. This allows us to impose the fluid dynamics analytically, so as to focus solely on the heat and mass transfer dynamics.

Hill's spherical vortex (Panton, 1984) is a classic solution to the Navier–Stokes equations, adapted by Hadamard and Rybcynski for the rising under buoyancy of small bubbles, with sufficiently strong surface tension, so that the bubble surface is undeformed from a sphere. Typically, this approximation is very good for bubbles of a few hundred microns or smaller in diameter. The internal velocity field is given by

$$v_z = U_t\left(1-\left(\frac{z}{R}\right)^2-2\left(\frac{r}{R}\right)^2\right), \quad v_r = U_t\frac{r}{R}\frac{z}{R}, \quad U_t = \frac{1}{3}\frac{gR^2}{\mu}\Delta\rho \tag{1}$$

where v_z and v_r are the axial (z) and radial (r) coordinates, R is the radius of the bubble, and U_t is the terminal velocity for rising under gravitational acceleration g in a surrounding liquid with viscosity μ, and density difference $\Delta\rho$.

The system of equations that must be solved comprises the transport equations for mass and heat.

$$\frac{\partial c}{\partial t} + v\cdot\nabla c = D\nabla^2 c \tag{2}$$

$$\frac{\partial T}{\partial t} + v\cdot\nabla T = \alpha\nabla^2 T \tag{3}$$

Clearly, these equations differ only because of the variables – c is the molar concentration of water and T is the temperature field – and parameters, where D is the molecular diffusivity and α is the thermal diffusivity of the humid air. A common assumption in gas–liquid interfacial dynamics is that the interface has "flashed" to equilibrium. In the case of humid air in contact with water, this assumption is equivalent to fixing the partial pressure of water to the saturation pressure at the interface temperature, i.e.

$$p_w|_{r^2+z^2=R^2} = p^*(T) \text{ hence } c|_{r^2+z^2=R^2} = c^*(T) \tag{4}$$

at the low pressures and high temperatures considered here, it is sufficient to use the ideal gas law to convert the partial pressure of water to the molar concentration of water, c. MacInnes et al. (2010, 2012) have studied distillation in microchannels. MacInnes et al. (2012) uses this equilibrium boundary condition, albeit for presumed locally isothermal conditions. To our knowledge, there are no other modelling studies of micronscale film dynamics with micronscale structures and flows. It should be noted that a more fundamental model based on kinetic theory (Frezzotti, 2011; Fujikawa et al., 2011) would require molecular dynamics scale simulations and a multi-scale model to accommodate the continuum dynamics of bubble and surrounding liquid, which is beyond the scope of a first approach to the problem and the modelling objectives as proposed here.

The complicated boundary condition is for the heat transfer

$$q = \hat{n}\cdot k\nabla T$$
$$q = h(T-T_\infty) - \dot{m}\Delta H_v(T) \tag{5}$$

Fourier's Law is adapted to compute the normal flux component, which is then equated to two contributions: Newton's Law of Cooling where h is the local heat transfer coefficient and T_∞ is the ambient temperature of the liquid far from the bubble; the latent heat of vaporization of water $\Delta H_v(T)$ at that temperature weighted by the evaporation rate $\dot{m}$ on the interface. This is equation (3.71) of Treybal (1980), with no latent heat of dissolution. It is analogous to the two film theory of mass transfer resistance of Lewis and Whitman (1924) for sensible heat transfer alone. It should be noted that although Eq. (5) is not fundamental, the only treatment of microscale distillation with heat and mass transfer effects (Lam et al., 2011) uses more traditional McCabe–Thiele diagrams for analysis, for which no kinetic effects are treated.

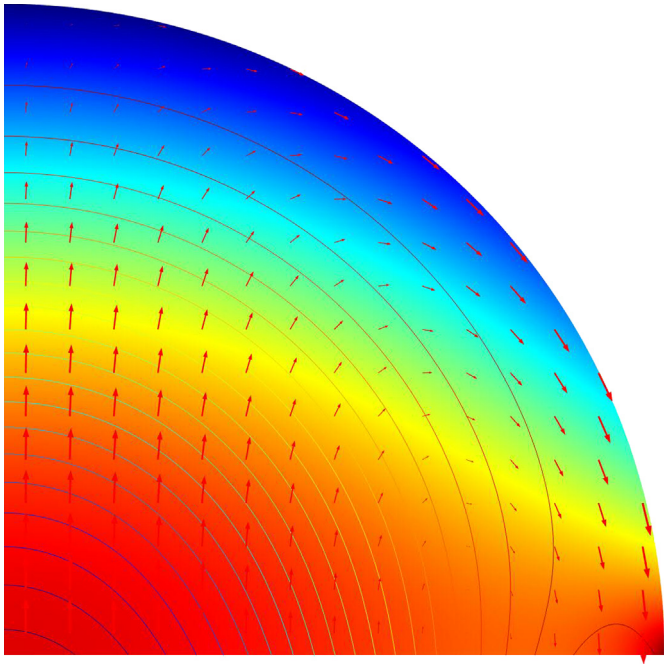

Fig. 2. Microbubble profile with $h=0.1$ W/m^2 K and $T_0=423$ K after $t=0.0001.5$ s with radius $R=100$ μm. The arrows are the induced, steady state velocity field from bubble rising, imposed as the velocity field of Eq. (1). The contours are isoconcentration curves, with 20 contours rising from 0.002 (inner) to 0.0032 (outer) molar concentration. The shading represents temperature, which is nearly isothermal at 315 K. This profile was selected as the maximum internal humidity was achieved.

In order compute the evaporation rate, we note that conservation of mass requires that the evaporative flux must equal the diffusive flux from the bubble surface inwards into the bubble interior:

$$\dot{m} = J = -\hat{n}\cdot D\nabla c \tag{6}$$

according to Fick's Law. The initial condition is that the bubble is injected with perfectly dry gas at $T=T_0$, uniformly in the gas phase.

2.2. Numerical analysis

Finite element Galerkin methods were used to compute the solutions to the model Eqs. (1)–(6) with a uniform inlet bubble temperature T_0 of perfectly dry gas ($c=0$) for a range of times, typically finishing at 1 s, where the bubble temperature is in equilibrium with the ambient temperature T_∞ far from the bubble. The domain is 2-D axisymmetric with a triangular mesh, generated by the elliptic algorithm, with 21,235 elements. Due to axisymmetry and spherical symmetry, the dynamics can be computed in a circular disc sector of the first quadrant in the r–z plane. A typical profile, computed in Comsol Multiphysics (see Zimmerman, submitted for how to set up such a model computation) of bubble humidity distribution, temperature field, and velocity vectors are shown in Fig. 3.

Physical properties are tabulated in Table 1. Thermal conductivity, heat capacity and hence thermal diffusivity, as well as the latent heat of vaporization, are considered as temperature dependent, and hence are varied according to a polynomial empirical correlation. As the temperature variation in Fig. 2 is not significant across the bubble, little error is introduced in not considered the spatial variation of the thermal conductivity in Eq. (2). Liquid and moist gas density, molecular diffusivity, and liquid viscosity are taken as constant. The most difficult parameter to assess is the heat transfer coefficient for the bubble. Kumar et al. (1992) measured the additional heat transfer coefficient from a rising bubble with ~1 cm radius and found it to be 1080 W/m^2 K. As our

bubble radius is 100-fold smaller, with 10^4 less surface area, we have taken $h=0.1$ W/m^2 K as an estimate. The issue of the appropriateness this choice is explored in Sections 2.5 and 3, with parametric variation investigated in Section 2.2.

Fig. 2 shows the most non-typical concentration profile, with maximum humidity on the skin, due to the choice of $t=1.5\times10^{-4}$ s, as the absolute humidity of the bubble passes through its maximum. The concentration time profile is complicated, as at long times, the lowest contours are actually near the skin of the bubble, as the average temperature profile largely decreases with time. Fig. 3 shows that the average temperature profile drops dramatically, at short times, due to the dominance of evaporation. Fig. 4 shows that there is an internal maximum in average humidity occurs that occurs at a very short time.

The bubble averaged temperature profile in Fig. 3 makes perfectly clear that there are two regimes: a rapid drop in

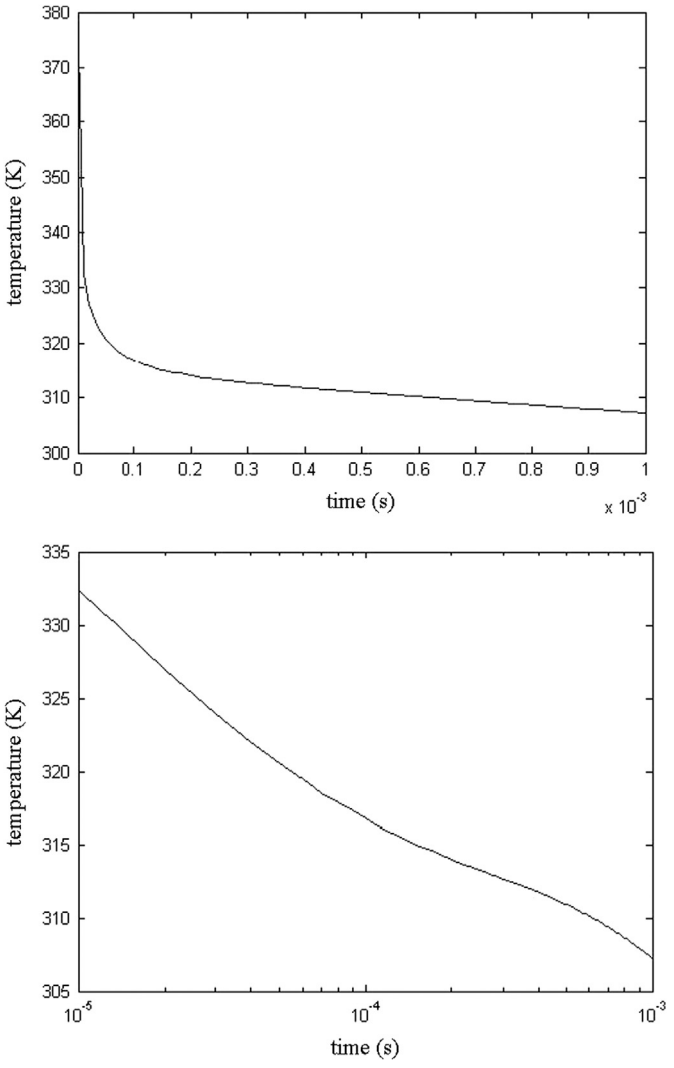

Fig. 3. Average bubble temperature vs. time (seconds) for a bubble with $T_0=423$ K initial temperature. Bottom: semilogx plot shows exponentially faster decay up to 10^{-4} s compared with the next 10^{-3} s.

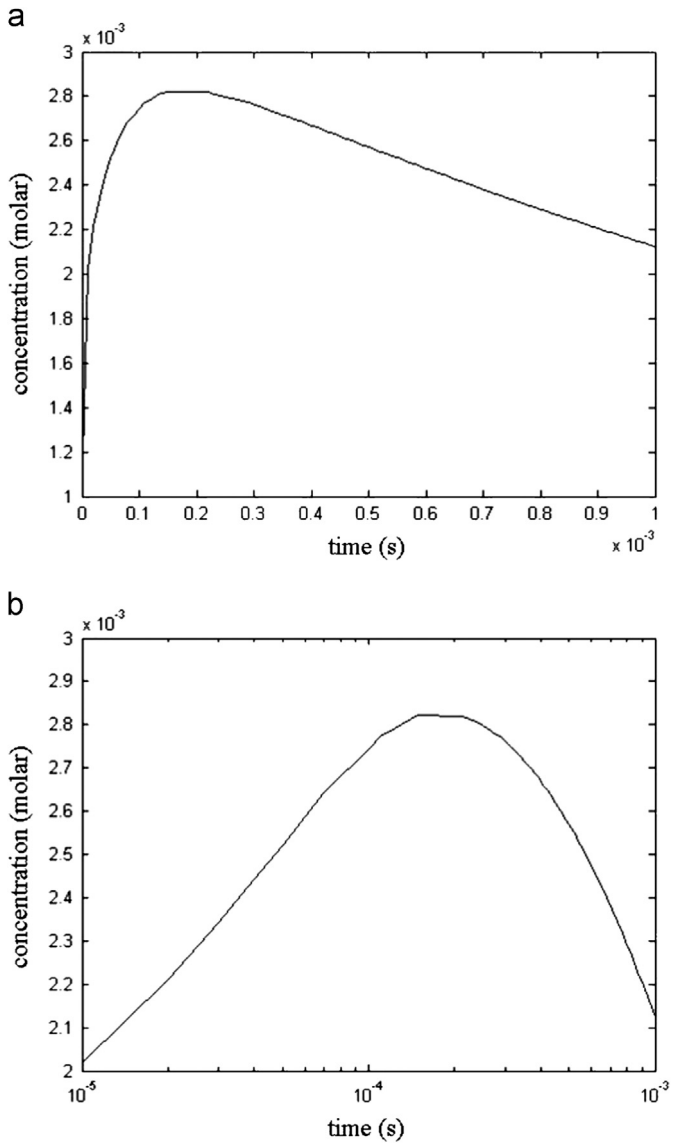

Fig. 4. Average bubble concentration (mol/liter) vs. time(sec) for a bubble with $T_0=423$ K initial temperature with $h=0.1$ W/m^2 K.

Table 1
Physical properties for the humification of a hot air bubble rising in room temperature water. (Felder and Rousseau, 1978).

Quantity	Value
Air density ρ (assumed T-independent)	1.2 kg/m^3
Liquid viscosity μ (25 °C)	8.9×10^{-4} kg/m/s
Liquid density ρ (25 °C)	1000 kg/m^3
Gas molecular diffusivity D	1×10^{-5} m^2/s
Thermal conductivity of moist air	0.00705852+5.78057 × 10^{-5} T+1.97511210^{-8} T^2 kg m/s^3
c_p (air)	28.09+0.1965 × 10^{-2} T+0.4799 × 10^{-5} T^2−1.965 × 10^{-9} T^3 kg m^2/s^2/mol/K
ΔH_v 25 °C	4.0656×10^4 kg m^2/s^2/mol
c_p (water vapour)	33.46+0.688 × 10^{-2} (T−273)+0.7604 × 10^{-5} (T−273)^2−3.593 × 10^{-9} (T−273)^3 kg m^2/s^2/mol/K
c_p (water)	75.4 kg m^2/s^2/mol/K
p^*	0.0075 × 10\widehat(7.96999−1670.45/(−44.7638+T)) Pa
c^*	p^*/RT; molarity

temperature with an inflection point at about $T=315$ K, followed by a slow decay towards the far field liquid temperature T_∞. We could speculate that evaporation dominates the first regime, and sensible heat transfer the latter. The semilog plot in Fig. 3 shows that evaporative cooling does happen at a rate approximately at least an order of magnitude more rapidly than sensible heat transfer.

Fig. 4 is the key graphic. It shows clearly that there is a quickly achieved maximum in absolute humidity with bubble rise time. With $R=50$ μm, the rise time according to the Hadamard–Rybcynski law is 0.0092 m/s, hence the maximum occurs on the order of one or at most a few bubble rise lengths. Thereafter, as sensible heat transfer cools the bubble, re-condensation must accompany it.

Fig. 5 shows an easily computable quantity ($\langle c(T)\rangle/c^*(\overline{T})$) that is a good estimate for the average relative humidity in the bubble, which shows that after the bubble achieves its maximum humidification, the relative humidity is constant (and fully saturated) as the bubble cools and condenses. Fig. 6 contains roughly complementary information—the bubble averaged evaporation rate is maximal initially and drops to a slightly negative rate (condensation) thereafter.

The only studies of microbubble mass transfer (Worden and Bredwell, 1998; Bredwell and Worden, 1998) have concluded that gas transfer dynamics are inherently transient. Fig. 4 shows that evaporation and heat transfer are inherently transient as well, and that maximum vaporization can be selected for with very small contact times, which translate into thin layers of just a few bubble diameters for the maximum absolute vaporization, and thereafter, sensible heat transfer dominates, so that higher layer thickness can be used to select for maximum heat transfer.

It is useful to define an effectiveness parameter for selective use of the excess enthalpy provided to a bubble for "paying" the latent heat of vaporization. A quantity with this connotation is defined by

$$\alpha = \frac{-c^*(T)}{N_{\text{tot}}/V}\frac{\Delta H_v(T)}{\int_{T_\infty}^{T_0} c_{p,\text{gas}}dT'} \tag{7}$$

where N_{tot} is the total moles of gas at a given time and V is the bubble volume. These quantities are assumed to be time invariant for simplicity of evaluation, so that α is a function of average bubble temperature only. α can be understood as the fraction of the additional enthalpy per unit volume of bubble introduced that results in vaporization. Fig. 7 shows the time variation of α for the specific case of Figs. 2–6, which illustrates three key features of its variation:

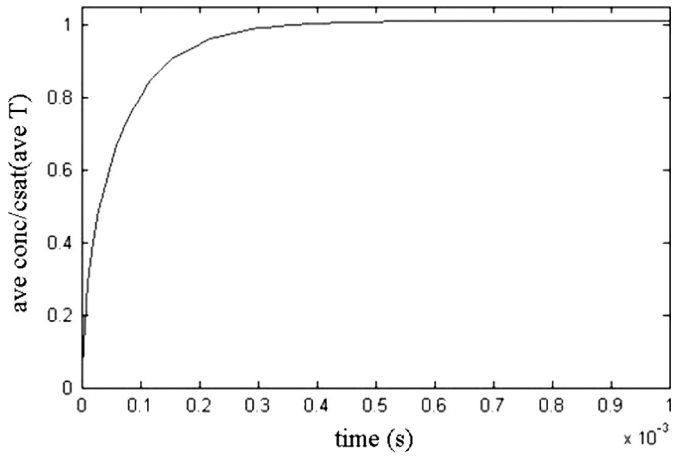

Fig. 5. Ratio of average water concentration to the saturated concentration at the average bubble temperature, vs. time (seconds) for a bubble with $T_0=423$ K initial temperature.

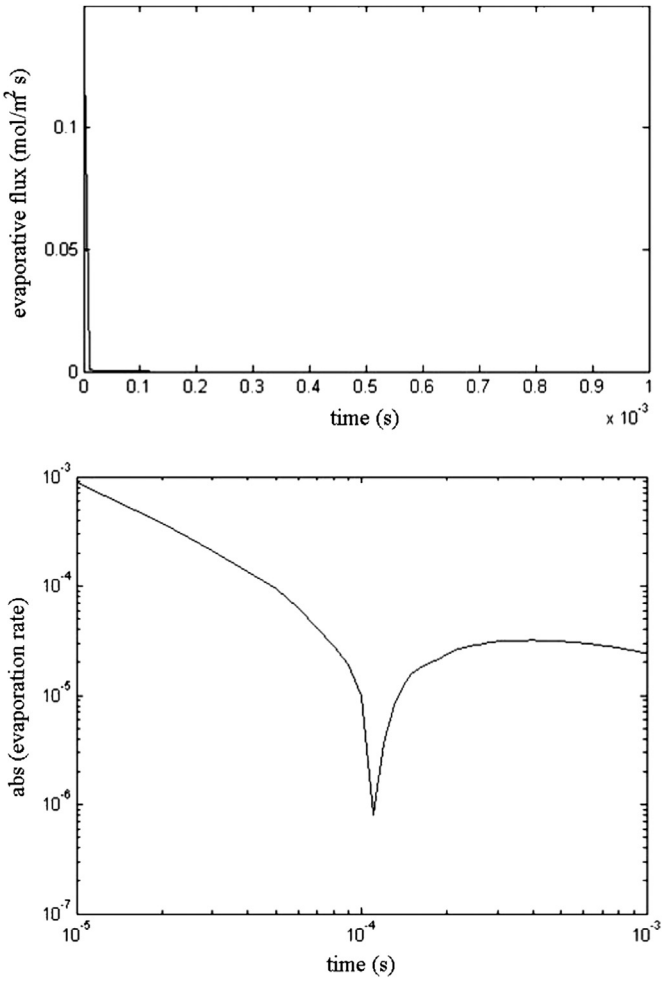

Fig. 6. Average evaporation rate (bubble skin mass flux) vs. time for bubble with $T_0=423$ K initial temperature. Bottom: log–log plot shows that at t~1.5×10^{-4} s, the bubble skin flux switches signs from evaporation to condensation.

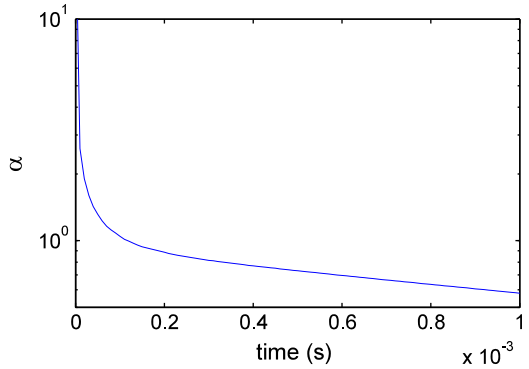

Fig. 7. Log-linear plot of the variation of α (ratio of latent heat used in evaporation to excess enthalpy in the bubble), defined in Eq. (7), over time for $h=0.1$ W/m^2 K, $R=0.0001$ m.

(i) $\alpha>1$ Since the bubble enters as perfectly dry air, initially evaporation includes the non-equilibrium mass transfer driver which pulls the latent heat of vaporization out of the *liquid* faster than it can use the excess enthalpy of the gas.
(ii) α~0.5 asymptotically as $t\to\infty$
(iii) $\alpha=1$ or $c=c_{\max}$ represents the greatest efficiency from the perspective of full use of the excess enthalpy charged to the injected bubble or greatest absolute humidity, and both of

these conditions occur, though not necessarily at the same contact time (see Table 3).

Although $\alpha > 1$ might superficially seem non-physical, there is no thermodynamic stricture stemming from the second law that prohibits a refrigeration effect. Indeed, this feature is observed experimentally in Zimmerman et al. (submitted for publication) for mixtures of methanol–water with bubbles that have insufficient excess enthalpy to vaporize to saturation – they draw the deficit in the latent heat of vaporization from the liquid itself!

2.3. Variation of heat transfer coefficient

The most uncertainty in the model concerns the heat transfer coefficient of a single microbubble. Although estimated here from single coarse bubble experiments of Kumar et al. (1992), the methodology for data assimilation with simultaneous experiment and modelling could be adapted to the humidification experiments using this model. The approach has been fully described by Zimmerman and Rees (2009) and implemented for heat and mass transfer coefficients in LNG storage tanks (Deshpande et al., 2011) and heterogeneous reactors with dispersed droplets for mass transfer coefficients (Deshpande and Zimmerman, 2005), as well as many microrheometer experiments (Rees and co-workers).

It is likely that the maximum vaporization level depends on the heat transfer coefficient, but it is unlikely that changes to this parameter estimate would change the key feature of Fig. 3, which is the post-maximum vaporization decline in absolute vaporization accompanied by sensible heating of the liquid and cooling of the bubble.

The previous models of heat and mass transfer dynamics for the formation and ascension of fine to coarse bubbles in direct contact evaporators Campos and Lage (2000a, 2000b, 2001) used the well known heat transfer analog to mass transfer and the Calderbank and Moo-Young (1961) correlation for "small bubbles" which in practice is limited to coarse bubbles. As discussed in Section 2.5, the heat transfer coefficient so estimated is substantially larger than that expected, on dimensional analysis grounds, for microbubbles. Section 3 experimentally supports the levels of h applied here.

Figs. 8 and 9 show the sensitivity of the time profiles of average bubble concentration and temperature to variation in the heat transfer coefficient. Because the long time scale behavior – transition to the condensation regime – is strongly dependent on the heat transfer coefficient, it was observed that transforming the time variable $t \to ht$ graphically collapses the range of concentration and temperature responses to within the same "interval" in ht,

Table 2
Variation of maximum absolute humidity and exponential temperature decay rate with heat transfer coefficient, with radius $R=50$ μm.

h (W/m^2 K)	t_{max} (s)	Max concentration $\bar{c}_{max}$ (mol/l)	α at $\bar{c}_{max}$	Decay constant τ (s)	Std. error estimate (s)
0.1	0.00006	0.00294	0.895	0.000149	0.000009
0.5	0.000032	0.00255	0.812	0.000032	0.000001
1	0.000018	0.00229	0.866	0.0000182	0.0000006
5	0.0000016	0.00168	2.28	4.78×10^{-6}	8.63×10^{-8}
10	0.0000006	0.00152	3.61	2.73×10^{-6}	4.40×10^{-8}

Table 3
Variation of maximum absolute humidity and exponential temperature decay rate with bubble size (and heat transfer coefficient).

R (m)	h (W/m^2 K)	t_{max} (s)	Max concentration $\bar{c}_{max}$ (mol/l)	α at $\bar{c}_{max}$	Decay constant τ (s)	Std. error estimate (s)
0.000025	0.00625	4.2×10^{-5}	3.21×10^{-3}	0.970	1.77×10^{-4}	6.89×10^{-6}
0.0005	0.03	9.0×10^{-5}	3.13×10^{-3}	0.951	2.94×10^{-4}	1.27×10^{-5}
0.0001	0.1	1.5×10^{-4}	2.82×10^{-3}	0.938	2.52×10^{-4}	1.99×10^{-5}
0.0002	0.4	1.9×10^{-4}	2.00×10^{-3}	0.949	1.38×10^{-4}	6.36×10^{-6}
0.0003	0.9	5.5×10^{-5}	1.57×10^{-3}	2.39	9.40×10^{-5}	3.35×10^{-6}
0.0006	3.6	1.6×10^{-5}	1.10×10^{-3}	9.35	9.42×10^{-5}	4.23×10^{-6}
0.001	10	1.6×10^{-5}	6.77×10^{-4}	13.7	6.99×10^{-5}	3.56×10^{-6}
0.01	1080	n/a	10^{-5}	n/a	n/a	n/a

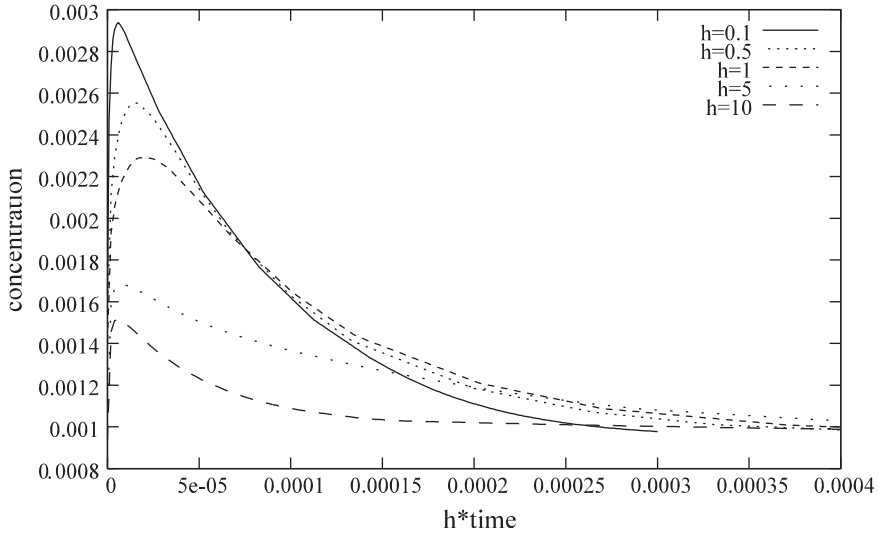

Fig. 8. Average concentration (mol/liter) variation time (seconds) profile with $h=0.1$ W/m^2 K (top), $h=0.5$, $h=1$, $h=5$, and $h=10$ (bottom). All curves have a maximum absolute humidity in the h*time interval [0.00001,0.00002], as tabulated in Table 2. The initial condition is "perfectly dry air" injected into the microbubble.

rather than ranging over two decades in actual time. A dimensional analysis would give a time-like dimensionless variable $\tau = ht/\rho_g c_{p,g} V$, but since the denominator is held constant in this subsection, it is clear that the dimensionless time variation emerges only through ht. Note that ht has units of J/m^2 K in Figs. 8 and 9.

Table 2 collates the information from five model computations with variation of the heat transfer coefficient, h, with profiles shown in Figs. 9 and 10. Although not obvious from Fig. 4, all the average temperature profiles, with the exception of an initial incubation period, are well described by an exponential decay function, with and empirically fitted decay constant τ:

$$\overline{T}(t) = T_\infty + (T_0 - T_\infty)\exp\left(-\frac{t}{\tau}\right) \quad (8)$$

From Table 2, it is clear that τ varies with heat transfer coefficient h, with but with a standard error of estimate that is two orders of magnitude smaller, indicative of a high level of confidence in its estimate. Clearly, the maximum absolute humidity $\overline{c}_{max}$, also varies strongly with h. With a fixed set of fluid physical parameters, bubble size and operating temperatures, these two emergent properties of the experiment appear to be highly sensitive to h, and monotonically varying. Hence, an estimate of either would be sufficient to infer h. In practice, constructing an experiment to measure the bubble humidity at the top of the liquid layer (known contacting time) or the temperature at the top of the layer is much easier than measuring either of these predicted quantities, but are likely to be difficult to attribute to the single bubble dynamics due to the mixing of heat and humidity in the header space. Since h is the bubble-to-liquid heat transfer coefficient, estimating the single bubble heat transfer coefficient may be easier from measuring the water temperature profile, with known bubble phase density and surface area.

2.4. Variation of bubble size

It is clear from Fig. 11 that with coarse bubbles, there is a "thin skin" around the bubble interface which is convected through the center/axis which is practically unheated and at near the liquid temperature. This thin skin surrounds a toroidal core which is practically unchanged in temperature from the initial injection. The fine bubble on the top of Fig. 10 is qualitatively thicker in its "skin", less broad in its hot core, and much better mixed—only 1.5 °C difference in the extremes. By comparison, the 50 μm diameter microbubble in Fig. 2 is for all intents uniformly mixed at a much earlier residence time.

Ubal et al. (2010) have conducted numerical simulations of buoyant droplet motion with mass transfer effects and have demonstrated that the boundary layer approach is consistent with no internal circulation, but that more rapid mixing occurs with internal circulation. Since both droplet and bubble motion are governed by the Hadamard circulation in microbubble regimes with laminar flow, the expectation with a nearly inviscid bubble (relative to a drop), is that internal mixing will exceed that of microdroplets of the same size. However, with coarse bubbles, the relative internal circulation is less intensive, so that Fig. 10 appears consistent with a rigid sphere/boundary layer penetration model.

2.5. Variation of inlet gas temperature

Fig. 12 shows the comparison of 8 average concentration profiles with variation of gas inlet temperature with the same liquid temperature and $R = 0.0001$ m and $h = 0.1$ W/m^2 K. The maximum concentrations are tabulated in Table 4. It is clear, however, that the low heat transfer coefficient for laminar flow results in a long plateau in concentration as re-condensation slowly progresses.

Table 4 shows that the maximum absolute humidity $\overline{c}_{max}$ rises rapidly with the inlet gas temperature T_0. Fig. 13 clarifies that this variation is linear in the initial temperature difference. It should be noted that since the latent heat of vaporization must be "paid", it is impossible to actually achieve $c^*(T_0)$, since vaporization lowers the gas phase temperature. The absolute humidity falls off from its maximum value more rapidly as the temperature driving force rises. With sufficiently long contacting time, the bubbles will achieve equilibrium at $T_\infty = 293$ K, i.e. 9.4×10^{-4} mol/l. Thus, Table 4 also shows that the maximum absolute humidity in this range of inlet gas temperatures ranges from ~*an order of magnitude higher* than expected from a bubble rising in a deep layer of water at room temperature. The additional vaporization achieved by heating the liquid with the same amount of sensible heat is guaranteed to be negligible, as $\rho\ c_p$ for water is 3 orders of magnitude larger than that for the vapour. Hence the same volume of water will change in temperature imperceptibly with this level of heating.

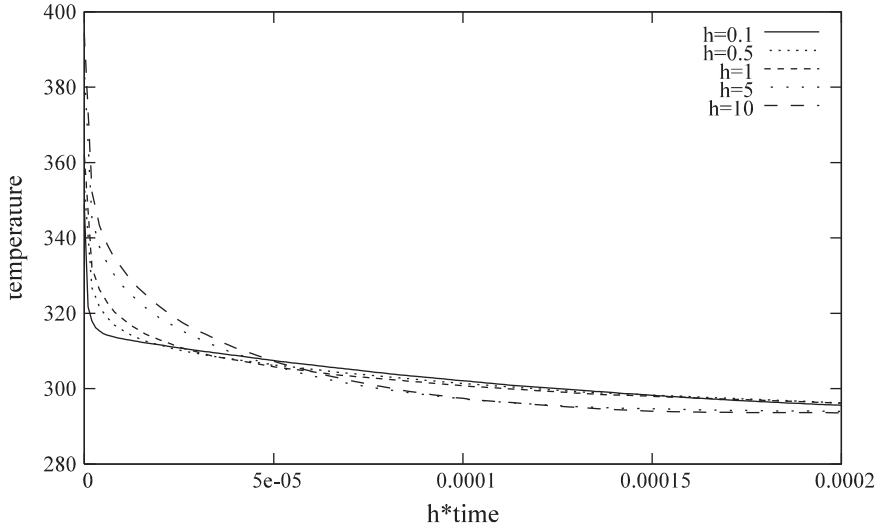

Fig. 9. Average temperature (K) variation time (seconds) profile with $h = 0.1$ W/m^2 K (top), $h = 0.5$, $h = 1$, $h = 5$, and $h = 10$ (bottom). The initial condition is "perfectly dry air" injected into the microbubble. The $h = 0.1$ profile has a clear break between two response time scales—an initial rapid drop during vaporization domination, followed by a slower, sensible heat transfer dominated regime with the release of the latent heat of vaporization by re-condensation.

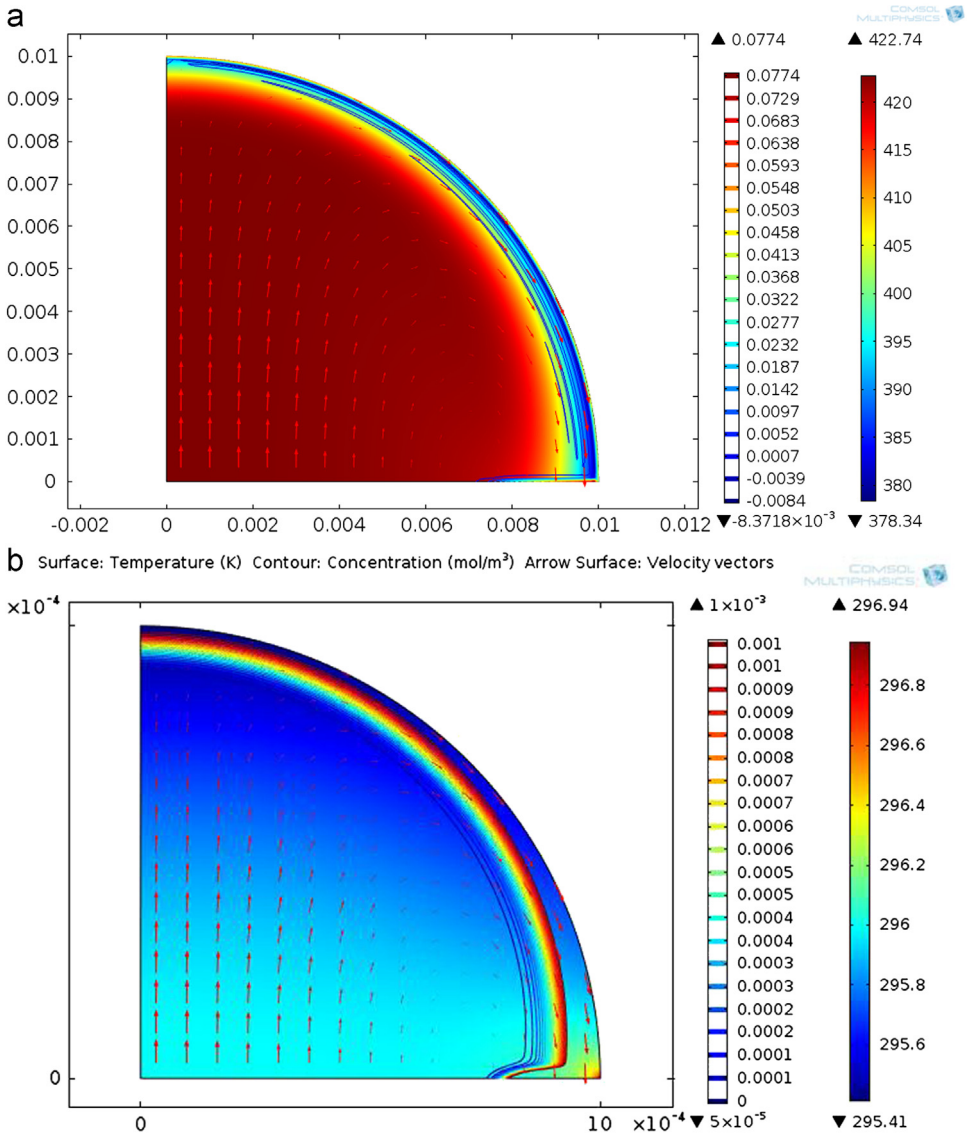

Fig. 10. Simulations of the flow field, concentration profile, and temperature distribution for both a fine (top) and coarse (bottom) bubble with $T_0=423$ K. (a) Flowfield, concentration profile, and temperature distribution with R=0.001m (fine bubble) after t=2×10^{-4}s and (b) Flowfield, concentration profile, and temperature distribution, R=0.01m (coarse bubble) after t=10^{-5}s.

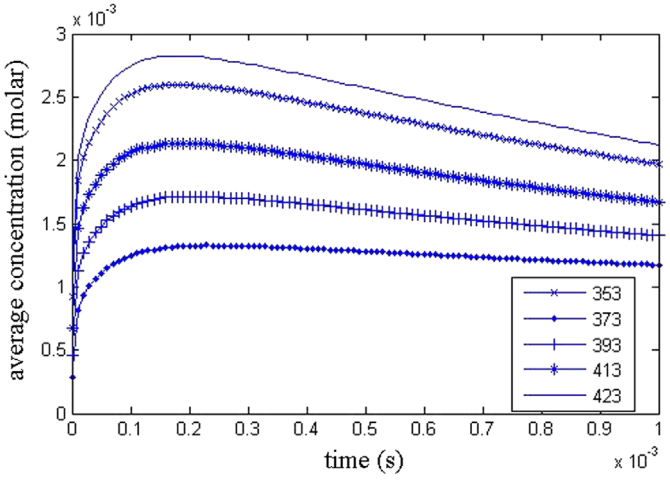

Fig. 11. Average concentration variation time profile with $T_0=353$ K (bottom), 363 K, 373 K, 383 K, 393 K, 403 K, 413 K, 423 K (top). All maximum absolute humidity is tabulated in Table 4. The initial condition was "perfectly dry air".

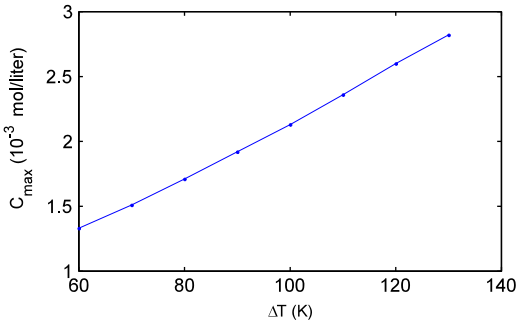

Fig. 12. Maximum concentration (10^{-3} mol/liter) variation against $\Delta T=T_0-T_\infty$. (°C). The initial condition was "perfectly dry air". The linear fit is $c_{max}=10^{-3}$ (mol/liter)$(0.00726+0.0215\,\Delta T)$.

2.6. Estimation of the heat transfer coefficient

In the preceeding computational modelling, we have taken the liquid-side heat transfer coefficient, h, to be a free parameter. This is justifiable if the bubbles are injected at a controlled rate with

significant excess kinetic energy, as, for instance, in the nucleation of small bubbles by saturated high pressure liquid injection into a low pressure liquid, such as in dissolved air flotation. But the target here is microbubbles rising under buoyancy only. Kumar et al. (1992) is the only direct study for the additional heat transfer due to a single bubble rising under buoyancy only that we could find in the literature, with $h=1080\ \mathrm{W/m^2\,K}$ the estimate for a coarse bubble of 2 cm diameter. Since we are miniaturizing the bubbles, it is reasonable to expect that the major contribution to heat transfer is convection, which would be expected to scale with a Peclet number,

$$Pe=\frac{U_t d}{\alpha}=\frac{1}{12}\frac{gd^3}{\mu\alpha}\Delta\rho \tag{9}$$

where α is the thermal diffusivity of the liquid, using the Hadamard drag law. Naively, if heat transfer were proportional to the Peclet number, then one would expect that h for a 200 μm diameter microbubble would be 6 orders of magnitude smaller than a 2 cm diameter coarse bubble. However, dimensional analysis is not respected by such a proportionality. The appropriate emergent dimensionless group is the Nusselt number, and similitude would imply

$$Nu=\frac{hd}{k}=f\left(\frac{gd^3}{\mu\alpha}\Delta\rho\right) \tag{10}$$

Table 4
Variation of maximum absolute humidity and exponential temperature decay rate with T_0 with fixed heat transfer coefficient $h=0.1$, liquid temperature $T_\infty=293$ K, and $R=100$ μ.

T_0 (K)	t_{max} (s)	Max concentration $\bar{c}_{max}$ (mol/l)	Decay constant τ (s)	Std. error estimate (s)
353	2.3×10^{-4}	1.33×10^{-3}	1.56×10^{-5}	2.29×10^{-6}
363	1.9×10^{-4}	1.51×10^{-3}	2.34×10^{-5}	3.47×10^{-6}
373	2.3×10^{-4}	1.71×10^{-3}	3.57×10^{-5}	5.12×10^{-6}
383	2.0×10^{-4}	1.92×10^{-3}	5.58×10^{-5}	7.34×10^{-6}
393	2.2×10^{-4}	2.13×10^{-3}	8.93×10^{-5}	1.03×10^{-5}
403	1.9×10^{-4}	2.36×10^{-3}	1.42×10^{-4}	1.40×10^{-5}
413	1.7×10^{-4}	2.60×10^{-3}	2.02×10^{-4}	1.74×10^{-5}
423	1.5×10^{-4}	2.82×10^{-3}	2.52×10^{-4}	1.99×10^{-5}

Although no functionality has been measured for microbubbles for the functional form f, Treybal (1980) reports a correlation for fine and coarse bubbles of

$$Nu=f(Pe)=0.6Pe^{1/2} \tag{11}$$

Working this correlation through yields

$$h\approx d^{1/2} \tag{12}$$

We have supposed that there are contributions to convective heat transfer with rising coarse bubbles due to the turbulence of the boundary layer for coarse bubbles rising which is absent in microbubbles, as well as the well known shape variation of deformable, large bubbles, which have size dependence through the Eotvos number

$$Eo=\frac{gd^2}{\sigma}\Delta\rho \tag{13}$$

See Grace et al. (1976) and Deshpande and Zimmerman (2006) for a description of deformation shapes with Eotvos and Reynolds number regimes. It is reasonable to imagine that in the microbubble regime, heat transfer is dominated by laminar flow, and hence

$$Nu\propto Pe \tag{14}$$

working such an ansatz through yields

$$h\approx d^2 \tag{15}$$

in the microbubble regime, which is 4 orders of magnitude smaller for 200 μm diameter microbubbles. Eventually, we would expect continued miniaturization would not yield any loss of heat transfer, as the convective mechanism would become dominated by heat conduction for practically non-buoyant microbubbles, such as the reported 5 μm size and smaller nanobubbles that do not rise (Zimmerman et al., 2011). Using these arguments, the parametric variation from 0.1 to 1080 $\mathrm{W/m^2\,K}$ span the likely range of heat transfer coefficients h.

2.7. A uniform theory for microbubble evaporation

Perhaps the most striking feature this study has is that, relatively speaking, microbubbles are well mixed after a very short

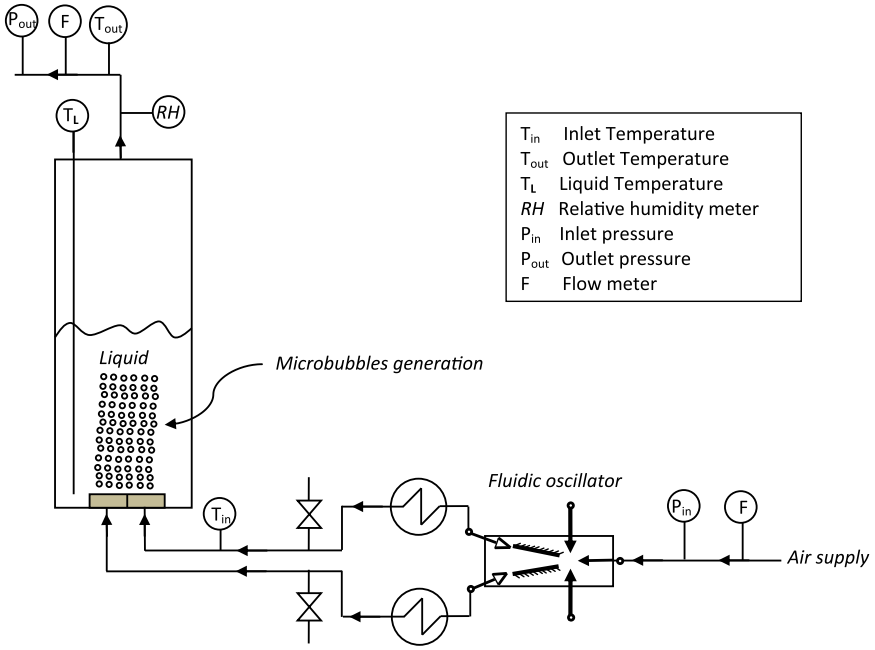

Fig. 13. Process flow diagram of the bubble column humidification and heat transfer unit.

evolution time. This is a direct consequence of the surface area to volume ratio and the Hadamard drag law—the slow rise rate is accompanied by a much larger relative surface traction to stir a smaller volume of gas. The comparison between Figs. 3 and 11 is striking—coarse bubbles and fine bubbles have a slowly stirred internal core, so that evaporation is essentially a boundary layer phenomenon. Because the surface renewal (Danckwerts, 1951) is so slow in fine and coarse bubbles, direct contact heating or evaporation does not typically result in complete use of the heat charged to a hot bubble for either aim.

Since microbubbles are well mixed after a short duration from injection, if they are assumed to have achieved the Hadamard terminal velocity upon injection, then a similar theory is possible to characterize the maximum possible vaporization state. We can compute the total amount evaporated from the time integration of the evaporation rate:

$$M = \int_0^t \dot{m}dt' = c^*(T)V \tag{16}$$

with the assumption of uniform concentration within the bubble permits the simplification to the last equality, where V is the volume of the assumed spherical bubble.

Let $Q_1 = \int_0^t qAdt'$ be the total amount of heat transferred to/from the bubble where A is the surface area of the bubble interface, and q is given by Eq. (5), hence

$$Q_1 = -hA(T-T_\infty)\Delta t - M\Delta H_v(T) \tag{17}$$

However, the overall heat balance shows that Q can also be computed by the enthalpy lost by the bubble:

$$Q_2 = \int_{T_0}^{T} N_{tot}c_p dT' \tag{18}$$

Ignoring the Laplace overpressure due to the surface tension (which for water is 0.14 Pa with $R=0.0001$ m), we can compute N_{tot} as a function of the pressure, bubble volume, and absolute temperature from the ideal gas law. Equating Q_1 and Q_2 gives a transcendental equation for the temperature, with the transcendental element coming from the temperature dependence of the saturation pressure of water.

For the values of Figs. 2–7, this works out at $t_{max}=1.5\times10^{-4}$ s with temperature at that contact time of $T=316.2$ K with $c^*(316\text{ K})=0.00332$ mol/l. These values are in good agreement with the $c_{max}=0.00294$ mol/l and $T_{max}=315$ K for the associated distributed model calculation reported in Table 2. It is also very near the smallest bubble performance reported in Table 3.

3. Heat transfer inference from microbubble cloud experimentation

The experiments that spurred this computational study were conducted in a purpose-built experimental rig with schematic as shown in Fig. 13. The flow diagram demonstrates that the gas temperature and flow rate at inlet to the bubble column heat transfer/humidity rig were controllable, and the bubble size could be influenced by the operation of the fluidic oscillator. In a recent study, Al-Mashhadani et al. (2012) reported that at the flow rates used here (operating conditions shown in Table 5), fluidic oscillation could vary the bubble size between 550 μm and 1.3 mm diameter, in this bubble column. The feedback loop length was 0.5 m, creating a frequency of ~100 Hz, but it is the whole fluidic oscillator-tubing-diffuser system that produces microbubbles, so the functionally important information is the average bubble size.

Table 6 shows that, in agreement with Fig. 6, the relative humidity was 100% at the gas outlet. Fig. 14 shows the liquid temperature history which rises with contacting of the room temperature water.

Table 5
Operating conditions for the bubble column heat transfer/humidification experiment.

Quantity of water (ml)	500 ± 1
Height of water in tank (cylinder)(mm)	45 ± 0.1
Flow rate of air inter to oscillator (L/min)	82 ± 2
Flow rate of hot air to diffuser (L/min)	3 ± 0.2
Flow rate of hot air bleed (L/min)	80 ± 2
Diameter of tank (mm)	140

Table 6
Key experimental measurements.

Relative humidity of inlet air	0%
Relative humidity of outlet air	100%
Volume before	500 ml
Volume after	466 ml
Volume of evaporated water	34 ml
Percentage evaporated water after 250 min (%)	6.8
Gauge pressure of inlet air (kPa)	50
Gauge pressure of outlet air (kPa)	0.716
Gas inlet temperature	145 °C

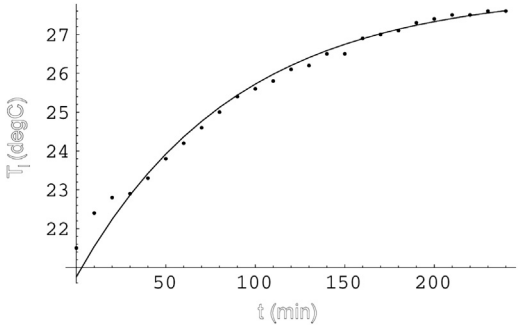

Fig. 14. Liquid temperature T_l in °C vs. time (min) for the bubble column. Dots are the experimental measure, and the curve is the best fit heat transfer coefficient $hA=0.4$ W/K and $T_g=28.1$ °C.

The curve fit in Fig. 14 was used to find the best estimates of the product of the heat transfer and surface area, as well as the skin temperature of the bubble phase T_g. The analysis follows classical heat transfer film theory. The total heat flux to the liquid must match the enthalpy gain of the liquid, hence

$$mc_p\frac{dT_l}{dt} = hA(T_g - T_l) \tag{19}$$

where m is the mass of the liquid, c_p is the heat capacity of the liquid, T_l is the liquid temperature, and A is the total bubble phase surface area. This differential equation can be solved analytically

$$T_g - T_l = Ce^{-\chi t} \tag{20}$$

where $\chi = hA/mc_p$. The best nonlinear regression fit gives ln $C=1.99$, $T_g=28.1$ °C, and $\chi=0.0113\text{ min}^{-1}$ with a correlation coefficient of 0.99. Substituting the known physical properties of water yields $hA=0.393\,W/K$. The standard errors of the parameter estimates were two orders of magnitude smaller. Presuming a 5% volume fraction of bubble phase holdup (40% porosity of the ceramic diffuser) and 600 μm diameter bubbles implies 0.225 m^2 of bubble phase surface area. Hence the estimate of the heat transfer coefficient is $h=1.2\,W/m^2K$. This is somewhat larger than the "base case" of $h=0.1$ W/m^2 K used in the simulations for

100 μm diameter bubbles, but shows that the computational model predictions have the correct trend and order of magnitude.

4. Discussion

Conventional microbubble clouds in industrial processes, such as dissolved air flotation (Edzwald, 1995), generate turbulent flow and intensive mixing, so that thermal equilibrium results from injecting microbubbles are rarely appreciably hotter than the surrounding liquid shortly after injection. Larger bubbles, such as the coarse bubbles injected in direct contact heating (Ribeiro and Lage, 2005; Francis and Pashley, 2009), also achieve thermal equilibrium when injected at higher rates than their terminal velocity. Hence, we would expect that the ratio of contact time to mixing time is crucial in determining the relative efficiency α of partition between vaporization and sensible heat transfer. Fig. 7 makes clear that long contact times relative to mixing times lead to α~0.5. But since conventional mechanisms of bubble cloud generation have short external mixing times due to turbulence, it has not previously be able to test the central hypothesis that α~1, or even $\alpha \gg 1$, is possible. Microbubble clouds in laminar flow have substantially lower heat transfer coefficients than expected from conventional small bubbles in turbulent flow, although intuitively expected, is demonstrated first here, with the unexpected consequence that α~1, or even $\alpha \gg 1$, is possible.

Perhaps it is instructive to consider the chronology of the formation of this hypothesis. There is a well known analogy between mass transfer and heat transfer, so we organized heat transfer coefficient estimates in the same experimental configuration of Zimmerman et al. (2008), which showed an 8-fold increase in oxygen transfer rates with 700 μm average bubbles generated with optimal frequency of fluidic oscillation, and ~10 mm bubble average size with steady flow. The expected result for heat transfer coefficient estimation would be an 8-fold increase with fluidic oscillation than without. With a sufficiently longer contact time than mixing time, the expectation of α~1, would lead to such a result. However, the result was an order of magnitude lower sensible heat transfer than expected, which led to the question of how to characterize the emergent level of humidification to complete the heat balance equation. The experiment of Section 3 was thus designed, with the ability to measure the humidity of the offgases, as well as to control the liquid level in a bubble column for which all of the vessel is sparged, so that the competiting processes of vaporization and sensible heat transfer could be characterized simultaneously.

In order to characterize the rate of evaporation, we expected to fit an evaporation rate law. For instance, Irving Langmuir (see Zemansky and Dittman, 1997) measured vapour pressures from evaporation from thin films and developed a kinetic theory based model for it. Inverting this model permits the prediction of evaporation rates from the subsaturated vapour pressure levels:

$$\dot{m} = \frac{\chi A(p^*(T_g) - P_v)}{\sqrt{2\pi(MW)RT_g}} \tag{21}$$

where χ is an effectiveness factor that is empirically fitted and MW is the molecular weight of the chemical species evaporated. Similarly to phenomenological approaches to non-equilibrium thermodynamics such as heat transfer and mass transfer, the flux is proportional to a driving force (deGroot and Mazur, 2011). Such first order systems are analogous to first order chemical reactions, for which tubular reactors can be used to estimate the rate constant. Zimmerman and Rees (2009) show how to estimate first order rate constants with convective mixing from reactor exit profiles, but the general rule is that the exit concentrations must not be at equilibrium, as that condition gives almost no information on the rate constant. It provides a lower bound on the rate constant, so if a reactor achieves equilibrium at the outlet concentrations, a plausible approach is to "cut" the reactor length in order to find a non-equilibrium outlet condition, from which a kinetic model can be fitted.

Conversely, the experimental work presented in Section 3, had the astounding result that *lowering* the liquid layer height, from 50 mm to 20 mm and then 10 mm, had the result of *increasing* the absolute humidity and outlet gas temperature, all with saturated offgases. If the analogy with reactor kinetics held, we would have expected eventually to find a non-equilibrium outlet condition so that a kinetic model, such as Langmuir's, might be fitted. However, "cutting the reactor length", i.e. lowering the liquid height, moved the outlet conditions further from thermal equilibrium. The intuitive view that evaporation and sensible heat transfer are competitive processes, motivated by observations of conventional processes with α~0.5, is not supported by the experiments. An alternative view, that, at least for microbubbles, the time scale for complete evaporation is very short relative to sensible heat transfer, is supported by the experiments, but not for coarse bubbles. The role of the transport model proposed here was to explain the experiments, which they do qualitatively, and in the case of liquid heat transfer coefficient, remarkably well quantitatively.

It is often conjectured, such as by Clift et al. (1978), that the interface of submillimeter bubbles, is blocked by surfactant impurities that are preferentially attracted to the interface due to their amphiphilic character. Such an interface would act as a hard sphere, and therefore have no slip, rather than the slip driving the internal motion. It would also block mass transfer across the interface. Indeed, Zimmerman et al. (2011) review the current theories for nanobubble stabilization, and it is the current view that impurities provide the stabilization through a complex of hydrogen bonding, that make nanobubbles relatively long-lived. However, there is a time scale for diffusion in liquids, and just about all solutes will diffuse in liquids with a molecular diffusivity of D~10^{-9} m^2/s, four orders of magnitude smaller than gas diffusion in a gaseous phase. Of course, the attraction of the surfactants to the interface represents a chemical potential driver, and within a laminar flow convection field. Nevertheless, the time scale for external surfactant mass transfer to the interface cannot exceed substantially the time scale for external heat transfer if both are convection dominated. Consequentially, the central conclusion here that the internal mixing time of the microbubble is sufficiently fast that evaporative mass transfer dominates heat transfer also permits the conclusion that it is faster than surfactant blockage of the interface to oppose mass transfer.

5. Conclusions

Direct contact evaporation has been around for years—sparging systems with hot gas to raise vapor. With energy efficient microbubble clouds, we have understood that it is possible *not to waste energy on sensible heat transfer if the target is raising vapour.* Because of the greater surface area per unit volume, *greater heat transfer* rates were intuitively expected. So *less* vaporization would be expected to occur with microbubbles due to less heat available for the latent heat of vaporization to be "paid". In fact, when conventional microbubbles are introduced with turbulent flow, the split of the energy introduced is equal between heat transfer to the liquid and the latent heat of vaporization. Nevertheless, direct contact evaporation is better than boiling, which heats the liquid and has heat losses that often exceed the heat given to vaporization.

Why do fluidic oscillator driven microbubbles achieve α~1, and even $\alpha \gg 1$? We introduce our bubbles gently into the liquid, with so much less energy density than conventional microbubbles that there is laminar flow around the bubbles. Hanotu et al. (2012) argues that the energy densities are 1000-fold smaller than the

nozzle exit regime for conventional saturation–nucleation microbubble generation. Heat transfer is slow, but vaporization is initially much faster. So by controlling the contact time, we can preferentially achieve much more effective vapourization with practically no sensible heat transfer to the liquid.

We have conducted experiments with a fully instrumented bubble column injecting hot, dry air into four different liquids—tap water, methanol-water and ethanol water binary mixtures, and a food stuff suspended in aqueous solution. These parallel studies will be reported in subsequent journal articles. Note that all experiments were conducted with sub-millimeter bubbles, with the smallest bubbles generated by fluidic oscillation. The major features of the experiments reported here, and supported with the subsequent binary mixtures, are:

- 100% relative humidity is always achieved.
- Vapour temperature *reduction* with contact time increase.
- Absolute humidity *decrease* with contact time increase.
- Higher liquid temperature with contact time increase.
- Greater than 95% selectivity for vaporization over sensible heat transfer achievable by tuning the layer height.

In addition to the industrial processes facilitated by direct contact evaporation conventionally, microbubble evaporation has several more potential applications:

- Dewatering/densification of liquids, potentially where temperature change would denature, cook, or spoil the substrate.
- Removal of volatile organic compounds, potentially where heat transfer would destabilize.
- Bioreactors with reactive extraction of volatile products, such as methane or ethanol.
- Low power consumption distillation of multicomponent liquids.
- Chemical synthesis with reactive extraction, such as condensation reactions (e.g. esterification).
- Desalination.

The experimental work that motivated this numerical study, partially presented in Section 3, had the astounding result that *lowering* the liquid layer height, from 50 mm to 20 mm and then 1 cm, had the result of *increasing* the absolute humidity and outlet gas temperature. This lead to the remarkable speculation that in the competition between vaporization and sensible heat transfer of the liquid element on the skin of the microbubble, the "race" is won immediately by vaporization. The liquid flashes to its equilibrium concentration of vapour on the surface layer. With coarse bubbles, this immediate flash has practically no importance, because the internal mixing of the bubble is too slow to take advantage from this preferential vaporization. With fine bubbles, as seen in Fig. 10, there is a modest effect as the internal mixing is stronger. With microbubbles, as seen dramatically in Fig. 2, the internal mixing dominates and there is a maximum absolute humidity achieved in a very short residence time, on the order of 10^{-3}s, according to Table 4. This equates to approximately one bubble length for the residence time to be achieved, so approximately a few hundred microns.

Acknowledgments

WZ would like to acknowledge support from the EPSRC (Grant no. EP/I019790/1). WZ would like to acknowledge the Royal Society for a Brian Mercer Innovation. MKAM would like to thank the Republic of Iraq for a doctoral scholarship. Many thanks also to Vaclav Tesar and Buddhi Hewakandamby for helpful discussions as well as Valentina Igenegbai and Brosk Ali for assistance. Assistance from Perlemax Ltd. on the commercial uses of direct contact evaporation is appreciated.

References

Al-Mashhadani, M.K.H., Hemaka Bandulasena, H.C, Zimmerman, W.B., 2012. CO_2 mass transfer induced through an airlift loop by a microbubble cloud generated by fluidic oscillation. Ind. Eng. Chem. Res. 51 (4), 1864–1877.
Bredwell, M.D., Worden, R.M., 1998. Mass-transfer properties of microbubbles. 1. Experimental studies. Biotechnol. Prog. 14 (1), 31–38.
Calderbank, P.H., Moo-Young, M.B., 1961. "The continuous phase heat and mass transfer properties of dispersions". Chem. Eng. Sci. 16, 39–54.
Campos, F.B., Lage, P.L.C., 2000a. Simultaneous heat and mass transfer during the ascension of superheated bubbles. Int. J. Heat Mass Transfer 43, 179–189.
Campos, F.B., Lage, P.L.C., 2000b. Heat and mass transfer modeling during the formation and ascension of superheated bubbles. Int. J. Heat Mass Transfer 43, 2883–2894.
Campos, F.B., Lage, P.L.C., 2001. Modelling and simulation of direct contact evaporators. Braz. J. Chem. Eng. 18 (3).
Clift, R., Grace, J.R., Weber, M.E., 1978. Bubbles, Drops and Particles. Academic, New York.
Danckwerts, P.V., 1951. Significance of liquid film co-efficient in gas absorption. Ind. Eng. Chem 43, 1460–1467.
de Groot, S., Mazur, P., 2011. Non-equilibrium Thermodynamics. Dover Publications, New York.
Deshpande, K.B., Zimmerman, W.B., 2006. Simulation of interfacial mass transfer by droplet dynamics using the level set method. Chem. Eng. Sci. 61, 6486–6498.
Deshpande, K.B., Zimmerman, W.B., 2005. Experimental study of mass transfer limited reaction. Part I: A novel approach to infer asymmetric mass transfer coefficients 60 (11), 2879–2893Chem. Eng. Sci. 60 (11), 2879–2893.
Deshpande, K.B., Zimmerman, W.B., Tennant, M.T., Webster, M.B., Lukaszewski, M.W., 2011. Optimization methods for the real-time inverse problem posed by modelling of liquefied natural gas storage. Chemical Engineering Journal 170 (1), 44–52.
Edzwald, J.K., 1995. Principles and applications of dissolved air flotation. Water Sci. Technol. 31, 1–23.
Felder, R.M., Rousseau, R.W., 1978. Elementary Principles of Chemical Processes. Wiley and Sons, New York.
Francis, M.J., Pashley, R.M., 2009. Application of a bubble column for evaporative cooling and a simple procedure for determining the latent heat of vaporization of aqueous salt solutions. J. Phys. Chem. B 113 (27), 9311–9315.
Frezzotti, A., 2011. Boundary conditions at the vapor–liquid interface. Phys. Fluids 23, 030609.
Fujikawa, S., Yano, T., Watanabe, M., 2011. Vapor–liquid interfaces, bubbles and droplets. Springer Heidelberg, Germany, Fundamentals and Applications, Series: Heat and Mass Transfer.
Grace, J.R., Wairegi, T., Nguyan, T.H., 1976. Shapes and velocities of single drops and bubbles moving freely through immiscible liquids. Trans. Ins. Chem. Eng. 54, 167–173.
Hanotu, J.O., Bandulasena, H.C.H, Zimmerman, W.B., 2012. Microflotation performance for algal separation. Biotechnol. Bioeng. 109 (7), 1663–1673.
Kumar, S., Kusakabe, K., Raghunathan, K., Fan, L.-S., 1992. Mechanism of heat transfer in bubbly liquid and liquid–solid systems: injection single bubble. AIChE J. 38 (5), 733.
Lam, K.F., Sorensen, E., Gavriilidis, A., 2011. Towards an understanding of the effects of operating conditions on separation by microfluidic distillation. Chem. Eng. Sci. 66, 2098–2106.
Lewis, W.K., Whitman, W.G., 1924. Principles of gas transfer absorption. Ind. Eng. Chem. 16, 1215.
MacInnes, J.M., Ortiz-Osorio, J., Jordan, P.J., Priestman, G.H., Allen, R.W.K., 2010. Experimental demonstration of rotating spiral microchannel distillation. Chem. Eng. J. 159, 159–169.
MacInnes, J.M., Pitt, M.J., Priestman, G.H., Allen, R.W.K., 2012. Analysis of two-phase contacting in a rotating spiral channel. Chem. Eng. Sci. 69, 304–315.
Narayan, G.P., Sharqawy, M.H., Summers, E.K., Lienhard, JH, Zubair, S.M., Antar, M.A., 2011. The potential of solar-driven humidification–dehumidification desalination for small-scale decentralized water production. Renewable Sustainable Energy Rev. 14, 1187–1201.
Narayan, G.P., Sharqawy, M.H., Lam, S., Das, S.K., Lienhard, J.H., 2013. Bubble columns for condensation at high concentrations of noncondensable gas: Heat-transfer model and experiments. AIChE J. , http://dx.doi.org/10.1002/aic.13944.
Panton, R.L., 1984. Incompressible Flow. John Wiley and Sons, NY.
Ribeiro, C.P., Lage, P.L.C., 2004a. Experimental study on bubble size distributions in a direct-contact evaporator. Braz. J. Chem. Eng. 21 (1), 69–81.
Ribeiro, C.P., Lage, P.L.C., 2004b. "Population balance modeling of bubble size distributions in a direct-contact evaporator using a sparger model". Chem. Eng. Sci. 59, 2363–2377.
Ribeiro, C.P., Lage, P.L.C., 2005. Gas–liquid direct-contact evaporation: a review. Chem. Eng Technol. 28 (10), 1081–1107.
Treybal, R.E., 1980. Mass-transfer Operations, 3rd Ed. McGraw-Hill, London.
Ubal, S., Harrison, C.H., Grassia, P., Korchinsky, W.J., 2010. Numerical simulation of mass transfer in circulating drops. Chem. Eng. Sci. 65, 2934–2956.
Worden, R.M., Bredwell, M.D., 1998. Mass-Transfer properties of microbubbles. 2. analysis using a dynamic model. Biotechnol. Prog. 14 (1), 39–46.

Zemansky, M.W., Dittman, R., 1997. Heat and Thermodynamics, 7th Ed. McGraw-Hill, New York.
Zimmerman, W.B., Rees, J.M., 2009. Optimal modelling and experimentation for the improved sustainability of microfluidic chemical technology design. Chem. Eng. Res. Des. 87 (6), 798–808.
Zimmerman, W.B., Václav Tesař, H.C., Hemaka Bandulasena, 2011. Towards energy efficient nanobubble generation with fluidic oscillation. Curr. Opin. Colloid Interface Sci. 16 (4), 350–356.
Zimmerman, W.B., Tesař, V., Butler, S.L., Bandulasena, H.C.H., 2008. Microbubble Generation. Recent Patents Eng. 2, 1.
Zimmerman, W.B., Hewakandamby, B.N., Tesař, V, Bandulasena, H.C.H., Omotowa, O.A., 2009. On the design and simulation of an airlift loop bioreactor with microbubble generation by fluidic oscillation. Food Bioproducts Process. 87, 215–227.
Zimmerman, W.B., Al-Mashhadani, K.H., Igenegbai Valentina, V.O., 2013. Cold boiling: fine and microbubble mediated binary distillation of methanol and water liquid solution. Phys. Chem. Chem. Phys. (submitted for publication).
Zimmerman, Al-Mashhadani and Igenegbai Valentina, Cold boiling: fine and microbubble mediated binary distillation of methanol and water liquid solution, Chem Eng Journal, accepted.